AGU ADVANCING EARTH AND SPACE SCIENCES

Geophysical Research Letters®

RESEARCH LETTER

10.1029/2025GL118510

Exceptionally Elongated Strike-Slip Rupture Caused by the 2025 M_W 7.8 Myanmar Earthquake

Quanshu Zhao[1], Guoyan Jiang[1], Yingwen Zhao[1], Xiaoping Hu[1], Lei Yang[1], Lingling Ye[2], Haipeng Luo[2], and Caijun Xu[1]

[1]School of Geodesy and Geomatics, School of Earth and Space Science and Technology, Wuhan University, Wuhan, China, [2]Department of Earth and Space Sciences, Southern University of Science and Technology, Shenzhen, China

Key Points:

- The 2025 Myanmar earthquake ruptured bilaterally, propagating northward at subshear speed and southward at supershear speed
- The Myanmar earthquake generated an exceptionally long, 472 km surface rupture, characterized by an extreme length-to-width ratio of 42
- The simple fault geometry and well-connected asperities likely facilitated the elongated rupture and southward supershear propagation

Supporting Information:

Supporting Information may be found in the online version of this article.

Correspondence to:

G. Jiang and Y. Zhao,
gyjiang@whu.edu.cn;
ywzhao@sgg.whu.edu.cn

Citation:

Zhao, Q., Jiang, G., Zhao, Y., Hu, X., Yang, L., Ye, L., et al. (2026). Exceptionally elongated strike-slip rupture caused by the 2025 M_W 7.8 Myanmar earthquake. *Geophysical Research Letters*, *53*, e2025GL118510. https://doi.org/10.1029/2025GL118510

Received 31 JUL 2025
Accepted 22 FEB 2026
Corrected 6 APR 2026

This article was corrected on 6 APR 2026. See the end of the full text for details.

Abstract The interplay between fault geometry and rupture behavior remains poorly understood. The 2025 Myanmar earthquake ruptured the Sagaing fault, a major continental strike-slip fault with simple geometry. We integrated geodetic and teleseismic observations to investigate its rupture process through finite-fault kinematic inversions and back-projection imaging. Our results show that the Myanmar earthquake ruptured bilaterally along the Sagaing fault, propagating southward from the hypocenter at a supershear speeds of 4.5–5.9 km/s and northward at a subshear speed of ~3.1 km/s, producing a 472-km-long surface rupture. The aspect ratio of the rupture length to width is up to 42, the largest value ever documented, likely due to simple fault geometry and well-connected asperities. The 2025 Myanmar earthquake, along with historical major events, reveals that the geometrically simple Sagaing fault exhibits variable rupture extent and recurrence intervals for large earthquakes due to fault segmentation.

Plain Language Summary Synthetic Aperture Radar observations of surface deformation reveal that the 2025 M_W 7.8 Myanmar earthquake ruptured a central section of the Sagaing fault spanning ~472 km. The rupture fault is characterized by a simple geometry, with a strike variation of only ~10°. Further analysis with geodetic and seismic observations indicates that the rupture occurred at depths shallower than 12 km, with a peak slip of up to 6.0 m. Comparison with global moderate-to-large strike-slip earthquakes since 1906 shows that the Myanmar event has the largest aspect ratio of rupture length to width, which is as high as 42, making it the most elongated strike-slip rupture in history. Although the Sagaing fault has a relatively simple geometry, it exhibits complex rupture behavior with large historical earthquakes showing both overlapping and non-overlapping rupture extents, as well as variable recurrence intervals.

1. Introduction

The potential for devastating earthquakes on active faults is typically assessed using seismic gaps inferred from geological evidence (e.g., McCann et al., 1979; Herman & Furlong, 2021; Plata-Martínez et al., 2021) or seismogenic asperities identified through geodetic and/or seismological observations (e.g., Bürgmann et al., 2000; Fialko, 2006). However, estimating the rupture lengths and magnitudes of potentially devastating earthquakes remains challenging because of the possibility of cascading ruptures involving multiple neighboring asperities (e.g., Gabriel et al., 2024; Lu et al., 2025; Ren et al., 2024). On 28 March 2025, a powerful earthquake with a moment magnitude (M_W) of 7.8 struck the Sagaing and Mandalay regions of Myanmar. It caused widespread destruction and significant casualties (Cai et al., 2025), marking it the deadliest event in the area since 1912 (Figure 1). The occurrence of the Myanmar earthquake was not entirely unexpected, as its epicenter lies near a well-defined seismic gap on the Sagaing fault (Wang et al., 2014; Xiong et al., 2017), which has remained quiet since 1839. However, the rupture extended much farther than anticipated, reaching nearly twice the length of the previously recognized gap (Hurukawa & Maung Maung, 2011; Peng et al., 2025; Ye et al., 2025).

The Sagaing fault is a major transform fault that accommodates more than half of the oblique convergence between the Indian and Sundaland plates (Tun & Watkinson, 2017; Zelenin et al., 2022; Lindsey et al., 2023, Figure 1). Although the fault extends up to ~1,500 km, its strike variation is minimal. In particular, the remarkably linear central section, spanning ~700 km from 17 to 23°N, exhibits a strike variation of only ~10°, which is substantially smaller than those (~30°–55°) of other large-scale strike-slip faults, such as the North and East Anatolian faults (Benjelloun et al., 2021; Wang & Barbot, 2024), the Great Sumatran fault (Sieh & Natawidjaja, 2000), the Altyn Tagh fault (Yang et al., 2024), and the Kunlun fault (Li et al., 2011). This makes it the

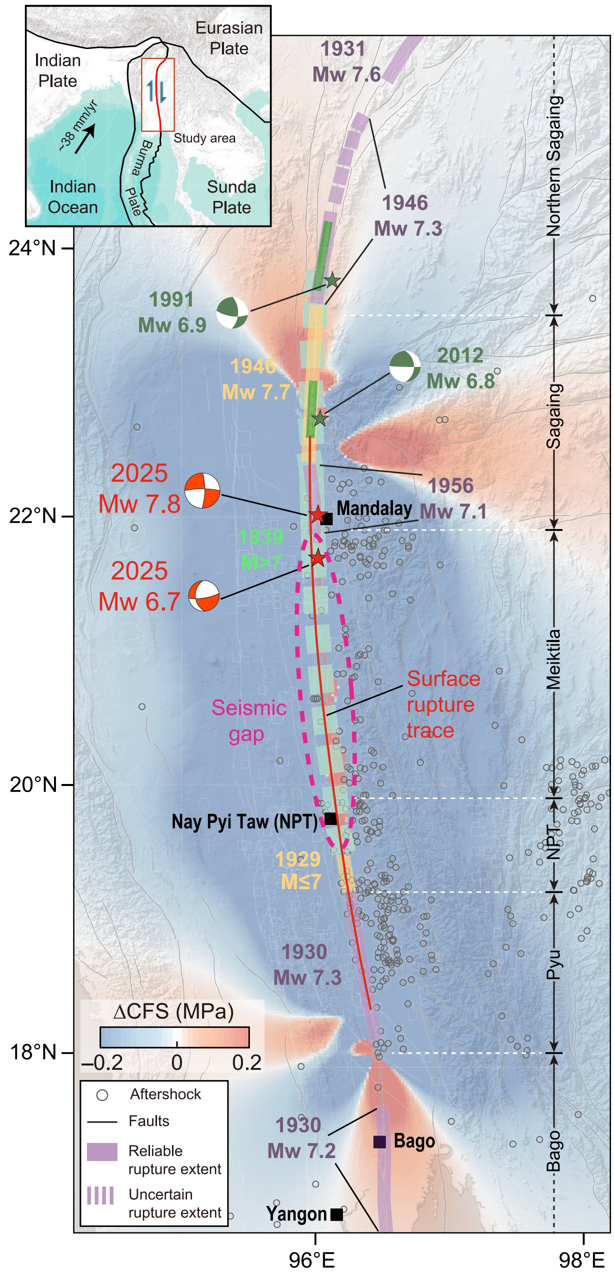

Figure 1. Seismotectonic background of the 2025 M_W 7.8 Myanmar earthquake. Two red stars denote the epicenters of the 2025 Myanmar earthquake and its largest aftershock. Green stars and green beach balls present the locations and focal mechanisms of two $M_W \geq 6.8$ earthquakes documented by the Global Centroid Moment Tensor catalog, with thick colored lines depicting their rupture extents (Wang et al., 2014). Gray circles show the aftershocks from the Thai Meteorological Department. Static Coulomb failure stress changes (ΔCFS) triggered by the 2025 M_W 7.8 Myanmar earthquake, assuming a friction coefficient of 0.4, are mapped by color shading. Active faults are shown by gray lines (Zelenin et al., 2022). Segmentation of the Sagaing fault was proposed by Wang et al. (2014). The top-left inset shows regional tectonic setting, with black lines delineating plate boundary faults and a black arrow indicating the motion of the Indian plate relative to Eurasia.

longest and most continuously linear strike-slip fault identified globally (Robinson et al., 2010). Due to high slip rates of 16–24 mm/yr (Lindsey et al., 2023), large-magnitude earthquakes have occurred frequently along the Sagaing fault with ten $M_W \geq 6.8$ earthquakes recorded over the past century (Figure 1).

Based on geomorphic and structural characteristics, as well as the rupture extents of paleo- and historical earthquakes, Wang et al. (2014) proposed that the central section of the Sagaing fault can be divided into five segments, that is, Sagaing, Meikatila, Nay Pyi Taw (NPT), Pyu, and Bago segments from north to South (Figure 1). Some segments have ruptured both individually and jointly with other segments, resulting in larger earthquakes (Wang et al., 2014). The Meiktila segment may represent an exception, with no record of independent rupture since 1839. The 2025 Myanmar earthquake not only ruptured the long-quiescent Meiktila segment, but also propagated northward to the Sagaing segment, which last failed in 1956, and southward into the NPT and Pyu segments, which last ruptured in 1929 and 1930, respectively (Tun & Watkinson, 2017; Wang et al., 2014).

Most previous studies have focused on mechanisms controlling the initiation and maintenance of supershear rupture, including simple fault geometry (e.g., Goldberg et al., 2025; Lindsey et al., 2023), high initial shear stress (e.g., He et al., 2026; Li et al., 2025), bimaterial effect (e.g., Antoine et al., 2025; Xu et al., 2025), and the presence of a thick low-velocity fault zone (Wei et al., 2025). However, another remarkable feature of this event—its exceptionally long rupture length—has received much less attention. In particular, it remains unclear whether the rupture conforms to conventional magnitude–length scaling relationships for strike-slip earthquakes (Wells & Coppersmith, 1994), and what physical factors may have enabled such an anomalously elongated rupture.

In this study, we investigated the Myanmar earthquake rupture with multiple Synthetic Aperture Radar (SAR) images and teleseismic waveforms. Our results show that the earthquake ruptured the central section of the Sagaing fault bilaterally, propagating southward at supershear speed and northward at subshear speed. Three major asperities failed during the event, producing the most elongated strike-slip rupture ever documented, with an exceptionally high length-to-width ratio. The occurrences of the Myanmar earthquake and other historical events on the Sagaing fault provide new insights into the rupture behaviors of large-scale strike-slip faults with simple geometry and underscore the need to reassess earthquake hazard models for such faults.

2. Coseismic Deformation Derived From SAR Images

We utilized pre- and post-earthquake C-band Sentinel-1 SAR images of two ascending and two descending tracks to measure surface deformation of the Myanmar earthquake. Interferograms were unwrapped to derive displacements in the line-of-sight (LOS) direction (more details refer to Supporting Information S1). However, the interferometric maps show significant phase decorrelation near the source fault (Figure S1 in Supporting Information S1), primarily resulting from large phase gradients induced by intense coseismic deformation and strong ground shaking that disturbed surface scatterers. To resolve near-fault deformation, we applied the pixel offset tracking technique (Michel et al., 1999) to identify shifts in pixel positions between the two SAR images of each track. The measured displacements in the range and azimuth

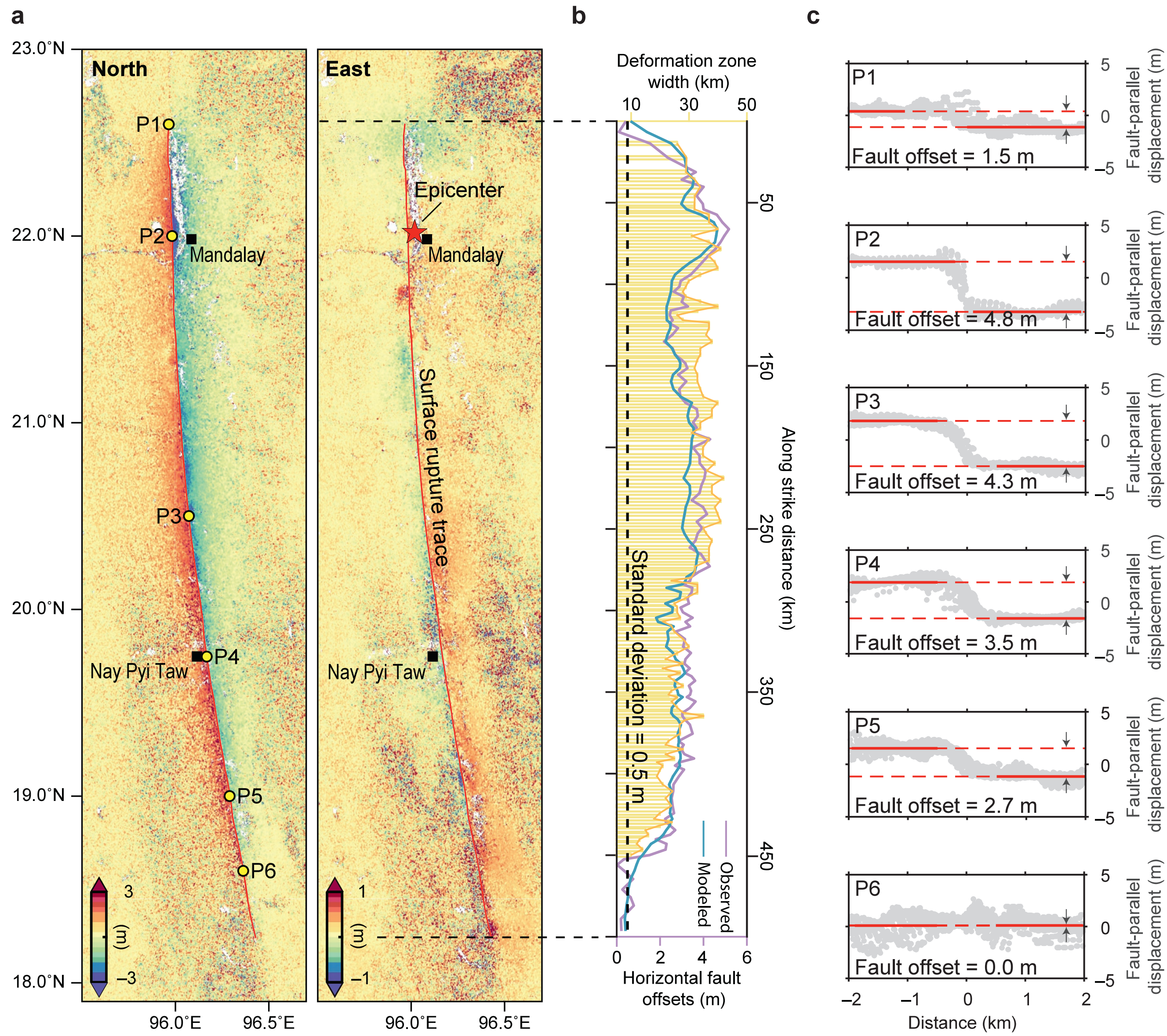

Figure 2. Surface deformation of the 2025 M_W 7.8 Myanmar earthquake. (a) Horizontal surface deformation derived from Synthetic Aperture Radar (SAR) images. The red line delineates the surface rupture trace. Yellow-filled circles display the positions of the six displacement profiles in panel (c). (b) Variation of off-fault extent of coseismic displacements (yellow bars and curve) along the fault. Purple and cyan curves show horizontal fault offsets measured by SAR observations and predicted by the finite-fault slip model in Figure 3a, respectively. The black dashed line indicates the standard deviation of horizontal deformation observations. (c) Six fault-parallel displacement profiles with measuring horizontal offsets. Red solid lines mark the average displacements on both sides of the fault, whereas red dashed lines correspond to their horizontal extensions.

directions clearly reveal an arc-shaped surface rupture (Figure S1 in Supporting Information S1), extending from north of Mandalay to south of NPT. However, the range offsets, which are mainly associated with east–west and vertical surface displacements, are much smaller than the azimuthal offsets, which primarily reflect north–south displacements.

The LOS displacements and pixel offsets of the four tracks were further combined to construct three-dimensional (3D) surface deformation maps with a resolution of 1 km by using the weighted least-squares method (more details refer to Supporting Information S1). The resulting northward displacement field clearly delineates the surface rupture trace, showing distinct offsets across the trace with a maximum magnitude of 4.9 m near Mandalay (Figure 2a). In contrast, the eastward and vertical deformation are only prominent in some localized regions

10.1029/2025GL118510

near the fault, with maximum values of 2.0 and 0.6 m, respectively (Figures 2a and Figure S3 in Supporting Information S1).

To evaluate the variation in deformation zone widths (i.e., the off-fault extent of coseismic displacements) and surface offsets along strike, we calculated fault-parallel (FN) displacements by projecting the eastward and northward displacement components onto the fault parallel direction in 240 profiles along fault strike. Each profile is oriented perpendicular to the fault strike and extends 400 km across the fault, including the FN displacements spanning 2 km along strike (Figures S4 and S15 in Supporting Information S1). We accounted for the width of the deformation zone by using locations with relative displacements exceeding 0.5 m, which is the observational uncertainty estimated from far-field measurements. The results show that the deformation zone widths range from 10 to 42 km with an average of 30 km (Figure 2b). We measure surface offsets across the fault using the profile of the FN displacements within 2 km on both sides across the fault (Figures 2c and Figures S16–S27 in Supporting Information S1). The average offset is 3.1 m, with a maximum value of up to 5.2 m near the epicenter. The deformation zone width scales with the amplitude of fault offset, with a correlation coefficient of 0.6 (Figure S28 in Supporting Information S1). Along the sections of the source fault where the offsets exceed 3 m, the deformation zones are over 24 km wide. We also identified the surface rupture where the offsets across the fault surpass the observational uncertainty. The surface deformation from Sentinel-1 SAR images shows that surface rupture of the 2025 M_W 7.8 Myanmar earthquake extends for 472 km (Figure 2b).

3. Rupture Model of the Myanmar Earthquake

3.1. Finite Fault Inversion Results

To image kinematic slip distribution of the 2025 M_W 7.8 Myanmar earthquake, we performed inversions with the observations of LOS displacements and pixel offsets. The observations were downsampled using the modified quadtree method proposed by Wang et al. (2022), who incorporated a topological analysis step to distinguish near-field from far-field measurements and applied two separate parameter sets for each observation group. The fault trace was simplified into five segments (red lines in Figure S2 in Supporting Information S1). We then constructed a 3D geometry of the seismogenic fault with triangular patches following the method developed by Jiang et al. (2013) to avoid dislocation gaps and overlaps, which can influence inversion results of slip distribution (Maerten et al., 2005). Slip on the patches was inverted by using the bounded variable least-squares algorithm (Stark & Parker, 1995). We also applied an iterative method to search for the optimal dip angles of the five segments during inversions (more details refer to Supporting Information S1). The best-fitting solution from the inversions show that the dip angle of the source fault increases along strike, from 60° near the hypocenter to 90° south of 18.8°N. The rupture is dominated by right-lateral strike slip, mainly at depths shallower than 12 km, with a peak slip of up to 6.0 m at depths of 4–6 km near the hypocenter (Figure 3a). Based on our preferred slip model, the earthquake has a seismic moment of 6.54×10^{20} N·m, with a shear modulus of 30 GPa, equivalent to M_W 7.8. The surface fault offsets predicted by our model show good spatial agreement with the SAR-measured results (Figure 2b).

The slip distribution at a depth of 5 km shows three distinct peaks with peak slip of ~5.6 m (Figure 3a). The 4 m slip contour delineates three major asperities (A1-A3). Asperity A1 is located between latitudes 21.9° and 22.4°N, with a length of ~64 km. It had ruptured during the 1839 $M > 7$ earthquake and partially ruptured during the 1946 M_W 7.7 and 1956 M_W 7.1 Sagaing earthquakes (Tun & Watkinson, 2017; Wang et al., 2014). Asperity A2 lies within the previously identified seismic gap, which has not ruptured since 1839, and measures about 100 km long and 8 km wide. Asperity A3 corresponds to the segments ruptured by the 1929 $M \leq 7$ Swa and 1930 M_W 7.3 Phyu earthquakes. The seismic moment for A1-A3 is 0.82×10^{20} N·m (M_W 7.2), 0.93×10^{20} N·m (M_W 7.3), and 0.72×10^{20} N·m (M_W 7.2), respectively. Overall, the 2025 Myanmar earthquake exhibits relatively continuous rupture without clear boundaries between these asperities, as confirmed by inversions with different smoothing factors (Figure S38).

3.2. Back-Projection Imaging Results

To gain insights into the dynamic characteristics of the 2025 Myanmar earthquake rupture, we adopted the multiple signal classification back-projection (BP) method (Meng et al., 2016) to resolve the location of high-frequency (HF) radiations recorded by the Alaska, European and Australia seismic networks (Supporting Information S1). The effect of velocity structure heterogeneity on the position of HF radiations was corrected by the

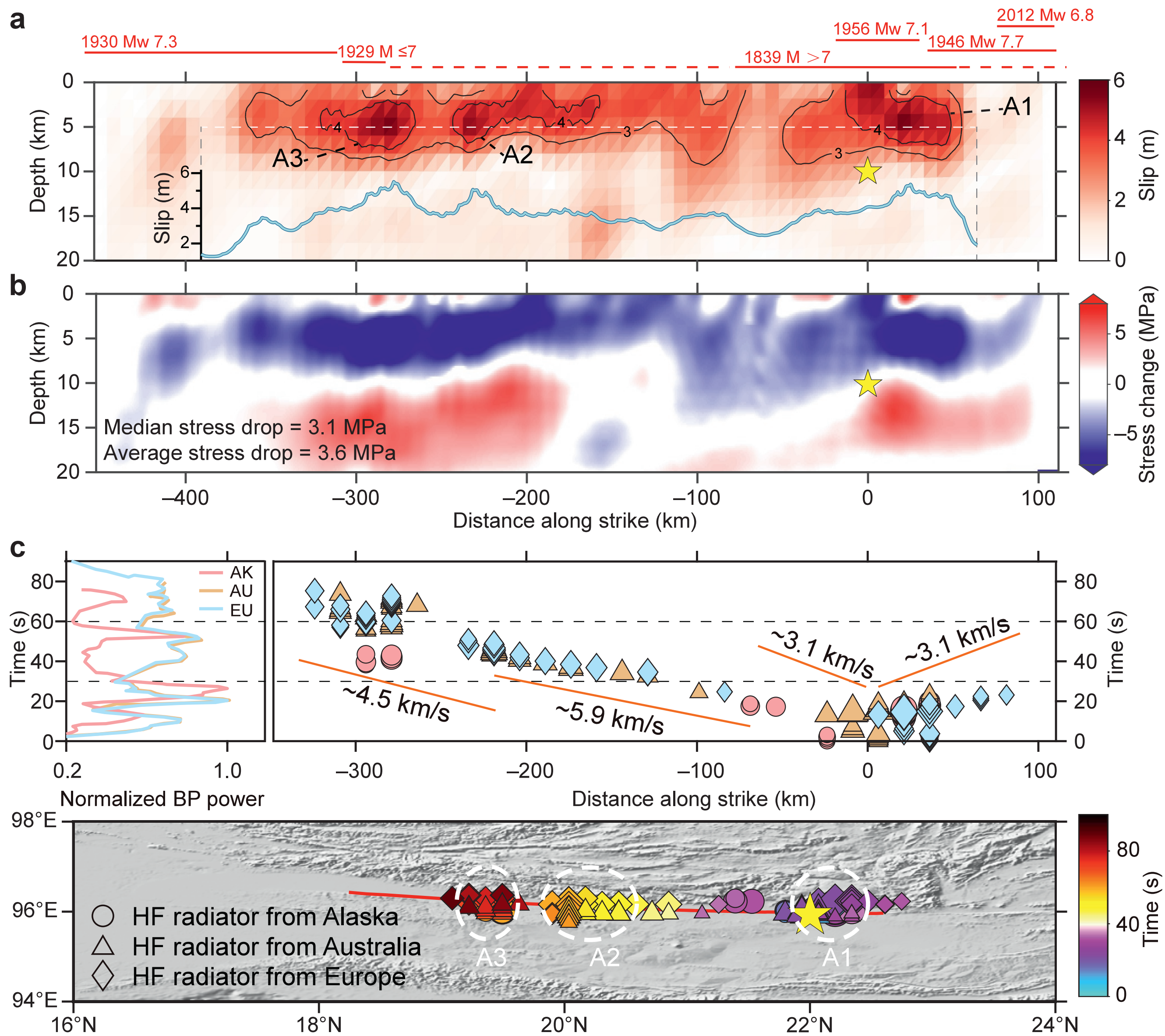

Figure 3. Rupture model of the 2025 M_W 7.8 Myanmar earthquake. (a) Finite fault slip model. The yellow star indicates the hypocenter. Black curves show the slip contours of 3 and 4 m, which outline the three major asperities (A1-A3). The blue curve represents the along-strike variation of slip at a depth of 5 km (the profile indicated by the dashed white line). Red solid and dashed lines show the rupture extents of historical $M_W \geq 6.8$ earthquakes (Wang et al., 2014). (b) Coseismic shear stress changes on the fault plane discretized with ~8 km^2 triangular patches. (c) Back-projection (BP) results from Alaska (AK), Australia (AU) and Europe (EU) arrays. The left panel shows normalized back-projection power release versus time. The right panel shows the temporal migration of coherent high-frequency (HF) (0.5–2 Hz) radiators from the epicenter along with estimated rupture speeds. The bottom panel shows the map view of HF radiations, color-coded by elapsed time with sizes scaled to the normalized BP power.

slowness-enhanced back-projection method (Bao et al., 2019), based on the slowness bias inferred from history earthquakes and aftershocks. The resulting HF radiation map shows a pronounced characteristic of bilateral rupture propagation along the source fault (Figure 3c), consistent with previous studies of this earthquake (Ding et al., 2025; Inoue et al., 2025; Vera et al., 2025; Ye et al., 2025). The northward rupture lasted for ~32 s at a subshear speed of ~3.1 km/s. In contrast, the southward rupture exhibited a three-stage supershear behavior, with rupture velocities ranging from 4.5 km/s to 5.9 km/s, lasting for ~80 s.

Comparison with the SAR-derived slip model reveals that the first-stage rupture occurred within and around asperity A1 from 0 to 30 s. The second stage, from 20 to 50 s and characterized by the fastest rupture speed of about 5.9 km/s, took place within the identified seismic gap where asperity A2 is located. The third-stage rupture, mainly within asperity A3, lasted for about 30 s. Moreover, the normalized BP power release exhibits four prominent peaks. The first and second peaks correspond to the bilateral rupture of asperity A1, while the third and fourth peaks are temporally associated with the ruptures of asperities A2 and A3, respectively. The power release from A1 is more abrupt than those from A2 and A3, likely reflecting more concentrated slip within A1.

4. An Exceptionally Elongated Strike-Slip Fault Rupture

To compare the aspect ratio of the rupture length to width of the 2025 Myanmar earthquake with other strike-slip events, we compiled a total of 175 strike-slip earthquakes globally from 1906 to 2025, with moment ranging from 4.1 to 8.6. Among them, 65 events between 1931 and 1992 are from Wells and Coppersmith (1994), with only rupture lengths (L) and widths (W) reported. For the other 110 events, we collected rupture length, width, and the minimum and maximum strike and dip angles from published source models (e.g., Lasserre et al., 2005; Ren et al., 2024; Song et al., 2008; Wei et al., 2013). We measured the rupture length and width for the region with slip exceeding 20% of the maximum slip (more details refer to Supporting Information S1).

The longest strike-slip rupture ever recorded was the 2012 M_W 8.6 Wharton Basin earthquake with a total along-strike rupture length of ∼740 km (Wei et al., 2013). However, this event involved the rupture of three conjugate faults. Among single-fault ruptures, the 1906 M_W 7.9 San Francisco earthquake is characterized by the longest rupture length of ∼480 km (Song et al., 2008). The 2025 Myanmar earthquake exhibits a rupture length comparable to that of the San Francisco event, but with a slightly smaller magnitude of M_W 7.8. The rupture lengths of the 175 earthquakes generally increase with magnitude, as expected by the empirical relationship proposed by Wells and Coppersmith (1994) (Figure 4a). Based on the newly compiled data set, our regression yields an updated log-linear scaling relation: $\log(L) = -2.63 + 0.64M_{W.}$ Although this updated relationship better fits the increasing trend in rupture length for large events, several events—including the 1906 San Francisco, 2020 Caribbean Sea (Tadapansawut et al., 2021), and 2025 Myanmar earthquakes—remain notable outliers (Figure 4b).

We further examined the relationship between aspect ratio and earthquake magnitude (Figure 4c). Eight events—including the 2025 M_W 7.8 Myanmar, 1992 M_W 7.9 San Francisco, Caribbean Sea, Kokoxili (Lasserre et al., 2005), 1958 M_W 7.8 Lituya Bay (Wells & Coppersmith, 1994), 1972 M_W 7.7 Sitka (Schell & Ruff, 1989), 1976 M_W 7.6 Motagua (Kanamori & Stewart, 1978), and 2023 M_W 7.8 Kahramanmaraş (Ren et al., 2024) earthquakes—have aspect ratios exceeding 15, with the 2025 Myanmar earthquake exhibiting the largest ratio (42). These earthquakes deviate markedly from the empirical scaling relationship, $\log(L/W) = -1.81 + 0.35M_W$ (Wells & Coppersmith, 1994, Figure 4c). Using the expanded data set, the improvement from the updated the scaling relationship in fitting the aspect ratios of these large-magnitude events remains limited (Figure 4c), implying that additional rupture mechanisms, such as supershear propagation (Bao et al., 2019; Ren et al., 2024) or complex fault interactions (Huang et al., 2025), may play a significant role in controlling large-magnitude earthquake rupture.

5. Discussion and Implications

5.1. Comparison With Published Rupture Models

Our slip model of the 2025 Myanmar earthquake is generally consistent with previously published models using seismic waveforms, SAR observations, or their combination (Table S6 in Supporting Information S1). The peak slips in our model and the other two models that also incorporate SAR observations are 6.0 m (Antoine et al., 2025; Wei et al., 2025), about 14%–25% lower than those obtained from joint inversions of seismic and geodetic data (Goldberg et al., 2025; Melgar et al., 2025; Xu et al., 2025). This discrepancy may arise from the inclusion of seismic observations, which can resolve short-duration, high-frequency slip and thereby yield larger peak-slip estimates (Wong et al., 2024), as well as from some effects of different model parameterization (e.g., fault discretization and slip smoothing constraints) employed for inversions (Ye et al., 2016). The second notable difference lies in the estimated seismic moments, which vary by roughly 3%–12% among the published models and our model. Such variations may reflect the influences of the adopted crustal velocity structures (e.g., homogeneous vs. layered velocity models), as well as from fault geometries (Melgar et al., 2025; Ye et al., 2025). In addition, slip in our model discretized with triangular patches is more continuous than in the rectangular-patch models, particularly near dislocation overlaps and gaps (Antoine et al., 2025; Goldberg

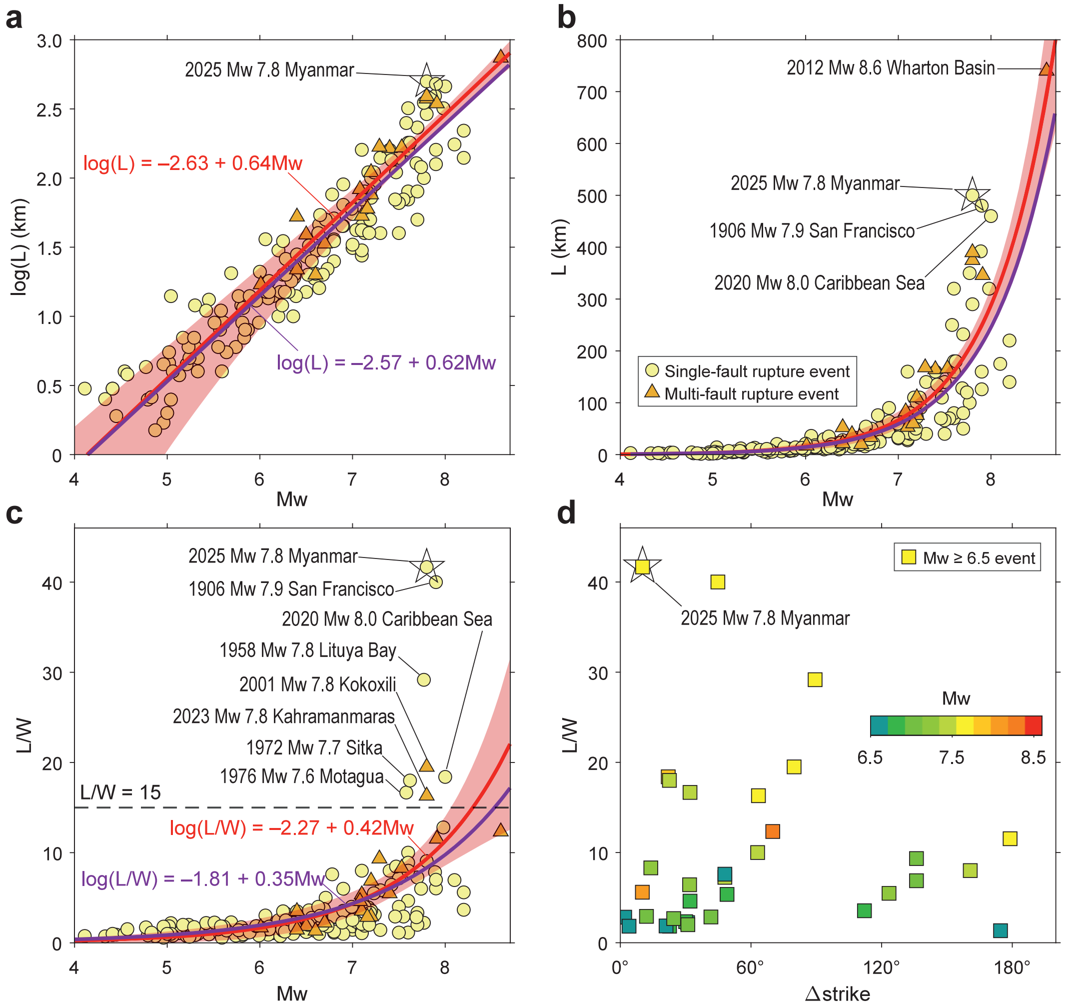

Figure 4. Statistical analysis of rupture geometry of 175 global strike-slip earthquakes (M_W 4.1–8.6) from 1906 to 2025. (a) Rupture length (L), plotted on a logarithmic scale, varies as a function of moment magnitude (M_W). Single- and multi-fault rupture events are shown as circles and triangles, respectively. The star shows the 2025 M_W 7.8 Myanmar earthquake. The purple curve shows the scaling relationship from Wells and Coppersmith (1994). The red curve indicates the updated empirical scaling relationship, with the pink shaded area representing the $\pm 1\sigma$ prediction band. (b) Variation of rupture length (L) with M_W. (c) Rupture aspect ratio (length to width, L/W) versus M_W. (d) Variation of aspect ratio with changes in fault strike during the rupture (maximum minus minimum strike) for earthquakes with magnitude larger than 6.5.

et al., 2025; Wei et al., 2025; Xu et al., 2025). For the BP results, our and previous studies show consistent rupture characteristics, including rupture duration, propagation speed, and rupture extent.

5.2. Possible Causes of the Extremely Elongated Rupture

The elongated rupture of the 2025 Myanmar earthquake may be related to the simple and nearly straight geometry of the source fault. The variation in the fault strike is only 10°, much less than those of the other $M_W > 7$ strike-slip events we compiled (Figure 4d). Geometric barriers like stepovers, bends, and intersections seem to be rare on the Sagaing fault (Table S7 in Supporting Information S1). Moreover, compared with faults characterized by complex geometries, simple and relatively straight faults like the Sagaing fault are more likely subjected to a laterally uniform prestress under a specific regional stress regime. These two factors have been demonstrated to promote both the onset and sustained propagation of supershear rupture (e.g., Bruhat et al., 2016; Day, 1982; He et al., 2026; Robinson et al., 2010), which can further facilitate the cascading rupture of multiple asperities, as observed in the 1906 San Francisco earthquake (Song et al., 2008), 2001 Kokoxili earthquake (Lasserre et al., 2005), and 2023 Kahramanmaraş earthquake doublets in Turkey (Ren et al., 2024). It is worth noting that, for the 2025 Myanmar earthquake, the asperities are well connected, particularly between the major asperities A2 and A3, which is also favorable for rupture propagation (Kato, 2004).

In addition, rupture propagation is also related to the coupled effects of stress drop and strength excess (defined as the difference between the fault's static strength and the dynamic stress during rupture propagation), with larger stress drops and smaller strength excesses facilitating rupture continuity across segment boundaries (e.g., Dunham, 2007; Li et al., 2025; Xu et al., 2015). For the Myanmar earthquake, the stress drops range from 0.02 to 11.8 MPa with average of 4.5 MPa along the segment where the rupture transitioned from subshear to supershear (Figure 3b). The peak stress drop is 14.7 MPa, located within the asperity A3. The averaged stress drop of the entire rupture is 3.6 MPa, comparable to those of other $M_W > 7.6$ strike-slip events (Allmann & Shearer, 2009; Cocco et al., 2016) and large subduction zone earthquakes (Ye et al., 2016). Therefore, we think that if the stress drop plays an important role in the elongated and supershear rupture (Bruhat et al., 2016; Dunham, 2007), the fault strength may need to be lower than in other major strike-slip faults favoring subshear events (He et al., 2026).

5.3. Implications for Seismic Hazards

The 2025 Myanmar earthquake, together with historical $M_W \geq 6.8$ events (Figure 1), reveals complex rupture behaviors of large-magnitude earthquakes along the central section of the Sagaing fault. The rupture extents for earthquake with different magnitudes exhibit both overlapping and non-overlapping scenarios. In overlapping scenarios, some fault sections have been ruptured during earthquakes with varying magnitudes. For example, the rupture segment of the 2012 M_W 6.8 earthquake also failed during the 1946 M_W 7.7 event and likely during the 1839 $M > 7$ event (Wang et al., 2014). These rupture behaviors indicate that the Sagaing fault is poorly segmented, which could make it challenging to estimate earthquake magnitudes and recurrence intervals for individual fault sections (Antoine et al., 2025; Wesnousky, 2006). In other words, despite its geometrically simple structure, the fault exhibits substantial variability in rupture extent and recurrence intervals. Therefore, new models are needed to more accurately assess seismic hazards along large-scale strike-slip fault systems with simple geometry.

In addition, our static CFS calculations show that the 2025 Myanmar earthquake caused significant Coulomb stress increases in four regions (Figure 1). Two of these are located at the northern and southern ends of the rupture. In the north, the region with ΔCFS $\geq$0.1 MPa encompasses the rupture zones of the 1946 M_W 7.3 Wuntho and 1991 M_W 6.9 Mogok earthquakes (Tun & Watkinson, 2017; Wang et al., 2014). In the south, the 1930 M_W 7.2 Bago earthquake has occurred within the stress-increasing region (Tun & Watkinson, 2017). The other two regions are situated east of the northern end and west of the southern end, respectively. The positive Coulomb stress perturbation in these regions may elevate the likelihood and advance the occurrence of future earthquakes.

Conflict of Interest

The authors declare no conflicts of interest relevant to this study.

Data Availability Statement

The Sentinel-1 SAR images are provided by the European Space Agency (https://dataspace.copernicus.eu/browser/) and mirrored at the Alaska SAR Facility (https://search.asf.alaska.edu/#/). The global seismic data are publicly available from the IRIS-DMC (https://ds.iris.edu/wilber3/find_stations/11952284). The finite fault slip inversion and figure generation were carried out using the software Tectonic Geodesy Application (TGA) (Fang et al., 2020). The scripts for downloading SAR images, 3D surface deformation fields, slip model, BP imaging results, and compiled data set of strike-slip earthquake ruptures are available at Zhao et al. (2025).

Acknowledgments

We would like to thank three anonymous reviewers for their careful review and constructive comments. We also benefited from helpful discussion with Huihui Weng. This work was funded by the National Natural Science Foundation of China (Grants 42072245, 42130101, 42204004 and 42574012).

References

Allmann, B. P., & Shearer, P. M. (2009). Global variations of stress drop for moderate to large earthquakes. *Journal of Geophysical Research*, *114*(B1), B01310. https://doi.org/10.1029/2008JB005821

Antoine, S. L., Shrestha, R., Milliner, C., Im, K., Rollins, C., Wang, K., et al. (2025). The 2025 Mw7.7 Mandalay, Myanmar, earthquake reveals a complex earthquake cycle with clustering and variable segmentation on the Sagaing fault. *Proceedings of the National Academy of Sciences*, *122*(33), e2514378122. https://doi.org/10.1073/pnas.2514378122

Bao, H., Ampuero, J. P., Meng, L., Fielding, E. J., Liang, C., Milliner, C. W. D., et al. (2019). Early and persistent supershear rupture of the 2018 magnitude 7.5 Palu earthquake. *Nature Geoscience*, *12*(3), 200–205. https://doi.org/10.1038/s41561-018-0297-z

Benjelloun, Y., De Sigoyer, J., Garambois, S., Carcaillet, J., & Klinger, Y. (2021). Segmentation and Holocene behavior of the middle strand of the North Anatolian Fault (NW Turkey). *Tectonics*, *40*(11), e2021TC006870. https://doi.org/10.1029/2021TC006870

Bruhat, L., Fang, Z., & Dunham, E. M. (2016). Rupture complexity and the supershear transition on rough faults. *Journal of Geophysical Research: Solid Earth*, *121*(1), 210–224. https://doi.org/10.1002/2015JB012512

Bürgmann, R., Schmidt, D., Nadeau, R. M., d'Alessio, M., Fielding, E. J., Manaker, D., et al. (2000). Earthquake potential along the northern Hayward fault, California. *Science*, *289*(5482), 1178–1182. https://doi.org/10.1126/science.289.5482.1178

Cai, J., Nan, X., Han, G., Deng, W., & Sun, L. (2025). Rapid report of the March 28, 2025 M_W 7.9 Myanmar earthquake. *Earthquake Research Advances*, *5*(4), 100396. https://doi.org/10.1016/j.eqrea.2025.100396

Cocco, M., Tinti, E., & Cirella, A. (2016). On the scale dependence of earthquake stress drop. *Journal of Seismology*, *20*(4), 1151–1170. https://doi.org/10.1007/s10950-016-9594-4

Day, S. M. (1982). Three-dimensional simulation of spontaneous rupture: The effect of nonuniform prestress. *Bulletin of the Seismological Society of America*, *72*(6A), 1881–1902. https://doi.org/10.1785/BSSA07206A1881

Ding, X., Xu, S., & Ye, L. (2025). Intermittent supershear rupture punctuated by barrier-induced stopping phase during the 2025 Mw 7.8 Myanmar earthquake: Evidence from near-fault strong motion observation. *Geophysical Research Letters*, *52*(23), e2025GL118863. https://doi.org/10.1029/2025GL118863

Dunham, E. M. (2007). Conditions governing the occurrence of supershear ruptures under slip-weakening friction. *Journal of Geophysical Research*, *112*(B7), B07302. https://doi.org/10.1029/2006JB004717

Fang, Z., Jiang, G., Xu, C., & Wang, S. (2020). A tectonic geodesy mapping software based on QGIS. *Geodesy and Geodynamics*, *11*(1), 31–39. https://doi.org/10.1016/j.geog.2019.08.001

Fialko, Y. (2006). Interseismic strain accumulation and the earthquake potential on the southern San Andreas fault system. *Nature*, *441*(7096), 968–971. https://doi.org/10.1038/nature04797

Gabriel, A. A., Garagash, D. I., Palgunadi, K. H., & Mai, P. M. (2024). Fault size-dependent fracture energy explains multiscale seismicity and cascading earthquakes. *Science*, *385*(6707), eadj9587. https://doi.org/10.1126/science.adj9587

Goldberg, D. E., Yeck, W. L., Hanagan, C. E., Atterholt, J., Kehoe, H., Reitman, N. G., et al. (2025). Ultralong, supershear rupture of the 2025 Mw 7.7 Mandalay earthquake reveals unaccounted risk. *Science*, *390*(6772), 458–462. https://doi.org/10.1126/science.ady3581

He, Z., Zhang, Z., Wang, X., Wang, Z., Sunilkumar, T. C., Xu, X., & Wang, R. (2026). Rupture dynamics of the 2025 Mw 7.7 Myanmar earthquake: A bilateral supershear rupture on unusually long fault superhighway. *Geophysical Research Letters*, *53*(1), e2025GL118023. https://doi.org/10.1029/2025GL118023

Herman, M. W., & Furlong, K. P. (2021). Triggering an unexpected earthquake in an uncoupled subduction zone. *Science Advances*, *7*(13), eabf7590. https://doi.org/10.1126/sciadv.abf7590

Huang, C., Xu, W., Bürgmann, R., Xie, L., Feng, G., Shan, B., et al. (2025). Heterogeneous strong asperities and tectonic complexity control irregular cascading ruptures. *Science Advances*, *11*(33), eadv6771. https://doi.org/10.1126/sciadv.adv6771

Hurukawa, N., & Maung Maung, P. (2011). Two seismic gaps on the Sagaing Fault, Myanmar, derived from relocation of historical earthquakes since 1918. *Geophysical Research Letters*, *38*(1), L01310. https://doi.org/10.1029/2010GL046099

Inoue, N., Yamaguchi, R., Yagi, Y., Okuwaki, R., Enescu, B., & Tadapansawut, T. (2025). A multiple asymmetric bilateral rupture sequence derived from the peculiar tele-seismic P-waves of the 2025 Mandalay, Myanmar earthquake. *Seismica*, *4*(1). https://doi.org/10.26443/seismica.v4i1.1691

Jiang, G., Xu, C., Wen, Y., Liu, Y., Yin, Z., & Wang, J. (2013). Inversion for coseismic slip distribution of the 2010 M_W 6.9 Yushu earthquake from InSAR data using angular dislocations. *Geophysical Journal International*, *194*(2), 1011–1022. https://doi.org/10.1093/gji/ggt141

Kanamori, H., & Stewart, G. S. (1978). Seismological aspects of the Guatemala earthquake of February 4, 1976. *Journal of Geophysical Research*, *83*(B7), 3427–3434. https://doi.org/10.1029/JB083iB07p03427

Kato, N. (2004). Interaction of slip on asperities: Numerical simulation of seismic cycles on a two-dimensional planar fault with nonuniform frictional property. *Journal of Geophysical Research*, *109*(B12). https://doi.org/10.1029/2004JB003001

Lasserre, C., Peltzer, G., Crampé, F., Klinger, Y., van Der Woerd, J., & Tapponnier, P. (2005). Coseismic deformation of the 2001 M_W 7.8 Kokoxili earthquake in Tibet, measured by synthetic aperture radar interferometry. *Journal of Geophysical Research*, *110*(B12), B12408. https://doi.org/10.1029/2004JB003500

Li, B., Jónsson, S., Suhendi, C., Liu, J., Li, D., Delorme, A., et al. (2025). Seismic gap breached by the 2025 M w 7.7 Mandalay (Myanmar) earthquake. *Nature Geoscience*, *18*(12), 1287–1295. https://doi.org/10.1038/s41561-025-01861-7

Li, C., Xu, X., Wen, X., Zheng, R., Chen, G., Yang, H., et al. (2011). Rupture segmentation and slip partitioning of the mid-eastern part of the Kunlun Fault, north Tibetan Plateau. *Science China Earth Sciences*, *54*(11), 1730–1745. https://doi.org/10.1007/s11430-011-4239-5

Lindsey, E. O., Wang, Y., Aung, L. T., Chong, J., Qiu, Q., Mallick, R., et al. (2023). Active subduction and strain partitioning in Western Myanmar revealed by a dense survey GNSS network. *Earth and Planetary Science Letters*, *622*(15), 118384. https://doi.org/10.1016/j.epsl.2023.118384

Lu, W., Ide, S., & Yue, H. (2025). Feature of cascading rupture frequently observed in northern California. *Communications Earth and Environment*, *6*(1), 167. https://doi.org/10.1038/s43247-025-02138-y

Maerten, F., Resor, P., Pollard, D., & Maerten, L. (2005). Inverting for slip on three-dimensional fault surfaces using angular dislocations. *Bulletin of the Seismological Society of America*, *95*(5), 1654–1665. https://doi.org/10.1785/0120030181

McCann, W. R., Nishenko, S. P., Sykes, L. R., & Krause, J. (1979). Seismic gaps and plate tectonics: Seismic potential for major boundaries. *Pure and Applied Geophysics*, *117*(6), 1082–1147. https://doi.org/10.1007/BF00876211

Melgar, D., Weldon, R., Wang, Y., Bato, M. G., Aung, L. T., Shi, X., et al. (2025). Supershear source model of the 2025 M7.8 Myanmar earthquake and paleoseismology of the Sagaing fault: Regions of significant overlap with past earthquakes. *Seismica*, *4*(2). https://doi.org/10.26443/seismica.v4i2.1771

Meng, L., Zhang, A., & Yagi, Y. (2016). Improving back-projection imaging with a novel physics-based aftershock calibration approach: A case study of the 2015 gorkha earthquake. *Geophysical Research Letters*, *43*(2), 628–636. https://doi.org/10.1002/2015GL067034

Michel, R., Avouac, J. P., & Taboury, J. (1999). Measuring ground displacements from SAR amplitude images: Application to the Landers earthquake. *Geophysical Research Letters*, *26*(7), 875–878. https://doi.org/10.1029/1999GL900138

Peng, Z., Lei, X., Wang, D., Si, X., Mach, P., Zhong, Q., et al. (2025). Mainshock rupture properties, aftershock activities and remotely triggered seismicity associated with the 2025 Mw7. 7 Sagaing fault earthquake in Myanmar. *Earthquake Research Advances*, *5*(4), 100413. https://doi.org/10.1016/j.eqrea.2025.100413

Plata-Martínez, R., Ide, S., Shinohara, M., García, E. S., Mizuno, N., Dominguez, L. A., et al. (2021). Shallow slow earthquakes to decipher future catastrophic earthquakes in the Guerrero seismic gap. *Nature Communications*, *12*(1), 3976. https://doi.org/10.1038/s41467-021-24210-9

Ren, C., Wang, Z., Taymaz, T., Hu, N., Luo, H., Zhao, Z., et al. (2024). Supershear triggering and cascading fault ruptures of the 2023 Kahramanmaraş, Türkiye, earthquake doublet. *Science*, *383*(6680), 305–311. https://doi.org/10.1126/science.adi1519

Robinson, D. P., Das, S., & Searle, M. P. (2010). Earthquake fault superhighways. *Tectonophysics*, *493*(3–4), 236–243. https://doi.org/10.1016/j.tecto.2010.01.010

Schell, M. M., & Ruff, L. J. (1989). Rupture of a seismic gap in southeastern Alaska: The 1972 Sitka earthquake (Ms 7.6). *Physics of the Earth and Planetary Interiors*, *54*(3–4), 241–256. https://doi.org/10.1016/0031-9201(89)90246-X

Sieh, K., & Natawidjaja, D. (2000). Neotectonics of the Sumatran fault, Indonesia. *Journal of Geophysical Research*, *105*(B12), 28295–28326. https://doi.org/10.1029/2000JB900120

Song, S. G., Beroza, G. C., & Segall, P. (2008). A unified source model for the 1906 San Francisco earthquake. *Bulletin of the Seismological Society of America*, *98*(2), 823–831. https://doi.org/10.1785/0120060402

Stark, P. B., & Parker, R. L. (1995). Bounded-variable least-squares: An algorithm and applications. *Computational Statistics*, *10*, 129.

Tadapansawut, T., Okuwaki, R., Yagi, Y., & Yamashita, S. (2021). Rupture process of the 2020 Caribbean earthquake along the Oriente transform fault, involving supershear rupture and geometric complexity of fault. *Geophysical Research Letters*, *48*(1), e2020GL090899. https://doi.org/10.1029/2020GL090899

Tun, S. T., & Watkinson, I. M. (2017). The Sagaing fault, Myanmar. In A. J. Barber, K. Zaw, & M. J. Crow (Eds.), *Myanmar: Geology, resources and tectonics* (pp. 413–441). The Geological Society of London. https://doi.org/10.1144/M48

Vera, F., Carrillo-Ponce, A., Crosetto, S., Kosari, E., Metzger, S., Motagh, M., et al. (2025). Supershear rupture along the Sagaing fault seismic gap: The 2025 Myanmar earthquake. *The Seismic Record*, *5*(3), 289–299. https://doi.org/10.1785/0320250025

Wang, B., & Barbot, S. (2024). Rupture segmentation on the East Anatolian fault (Turkey) controlled by along-strike variations in long-term slip rates in a structurally complex fault system. *Geology*, *52*(10), 779–783. https://doi.org/10.1130/G52403.1

Wang, S., Jiang, G., Lei, X., Barbour, A. J., Tan, X., Xu, C., et al. (2022). Three mw≥ 4.7 earthquakes within the changning (China) shale gas field ruptured shallow faults intersecting with hydraulic fracturing Wells. *Journal of Geophysical Research: Solid Earth*, *127*(2), e2021JB022946. https://doi.org/10.1029/2021JB022946

Wang, Y., Sieh, K., Tun, S. T., Lai, K. Y., & Myint, T. (2014). Active tectonics and earthquake potential of the Myanmar region. *Journal of Geophysical Research: Solid Earth*, *119*(4), 3767–3822. https://doi.org/10.1002/2013JB010762

Wei, S., Helmberger, D., & Avouac, J. P. (2013). Modeling the 2012 wharton basin earthquakes off-Sumatra: Complete lithospheric failure. *Journal of Geophysical Research: Solid Earth*, *118*(7), 3592–3609. https://doi.org/10.1002/jgrb.50267

Wei, S., Wang, X., Li, C., Zeng, H., Ma, Z., Shi, Q., et al. (2025). Supershear rupture sustained through a thick fault zone in the 2025 Mw 7.8 Mandalay earthquake. *Science*, *390*(6772), 468–475. https://doi.org/10.1126/science.adz2101

Wells, D. L., & Coppersmith, K. J. (1994). New empirical relationships among magnitude, rupture length, rupture width, rupture area, and surface displacement. *Bulletin of the Seismological Society of America*, *84*(4), 974–1002. https://doi.org/10.1785/BSSA0840040974

Wesnousky, S. G. (2006). Predicting the endpoints of earthquake ruptures. *Nature*, *444*(7117), 358–360. https://doi.org/10.1038/nature05275

Wong, J. W. C., Fan, W., & Gabriel, A. A. (2024). A quantitative comparison and validation of finite-fault models: The 2011 tohoku-oki earthquake. *Journal of Geophysical Research: Solid Earth*, *129*(10), e2024JB029212. https://doi.org/10.1029/2024JB029212

Xiong, X., Shan, B., Zhou, Y., Wei, S., Li, Y., Wang, R. J., & Zheng, Y. (2017). Coulomb stress transfer and accumulation on the Sagaing fault, Myanmar, over the past 110 years and its implications for seismic hazard. *Geophysical Research Letters*, *44*(10), 4781–4789. https://doi.org/10.1002/2017GL072770

Xu, J., Zhang, H., & Chen, X. (2015). Rupture phase diagrams for a planar fault in 3-D full-space and half-space. *Geophysical Journal International*, *202*(3), 2194–2206. https://doi.org/10.1093/gji/ggv284

Xu, L., Meng, L., Yunjun, Z., Yang, Y., Wang, Y., Hu, C., et al. (2025). Bimaterial effect and favorable energy ratio enabled supershear rupture in the 2025 Mandalay earthquake. *Science*, *390*(6772), 476–481. https://doi.org/10.1126/science.ady6100

Yang, H., Lin, D., Yang, X., Cunningham, D., Hu, Z., Huang, X., et al. (2024). Strain partitioning and strike-slip faulting in the nanjieshan, North Tibetan Foreland: Progressive widening of the Altyn Tagh Fault system with implications for regional earthquake hazards. *Tectonics*, *43*(12), e2024TC008262. https://doi.org/10.1029/2024TC008262

Ye, L., Lay, T., & Kanamori, H. (2025). The 28 march 2025 M_W 7.8 Myanmar earthquake: Preliminary analysis of an ∼480 km long intermittent Supershear rupture. *The Seismic Record*, *5*(3), 260–269. https://doi.org/10.1785/0320250021

Ye, L., Lay, T., Kanamori, H., & Rivera, L. (2016). Rupture characteristics of major and great (Mw ≥7.0) megathrust earthquakes from 1990 to 2015: 1. Source parameter scaling relationships. *Journal of Geophysical Research: Solid Earth*, *121*(2), 826–844. https://doi.org/10.1002/2015JB012426

Zelenin, E., Bachmanov, D., Garipova, S., Trifonov, V., & Kozhu-rin, A. (2022). The active Faults of Eurasia database (AFEAD): The ontology and design behind the continental-scale dataset. *Earth System Science Data*, *14*(10), 4489–4503. https://doi.org/10.5194/essd-14-4489-2022

Zhao, Q., Zhao, Y., Jiang, G., Hu, X., Yang, L., Ye, L., et al. (2025). Data and slip model of 2025 Myanmar earthquake [Dataset]. *Zenodo*. https://doi.org/10.5281/zenodo.15780002

References From the Supporting Information

Bassin, C., Laske, G., & Masters, T. G. (2000). The current limits of resolution for surface wave tomography in North America. *EOS Trans. AGU*, *81*, F897.

Chen, C. W., & Zebker, H. A. (2000). Network approaches to two-dimensional phase unwrapping: Intractability and two new algorithms. *Journal of the Optical Society of America*, *17*(3), 401–414. https://doi.org/10.1364/JOSAA.17.000401

Comninou, M., & Dundurs, J. (1975). The angular dislocation in a half space. *Journal of Elasticity*, *5*(3), 203–216. https://doi.org/10.1007/BF00126985

Doin, M. P., Lasserre, C., Peltzer, G., Cavalié, O., & Doubre, C. (2009). Corrections of stratified tropospheric delays in SAR interferometry: Validation with global atmospheric models. *Journal of Applied Geophysics*, *69*(1), 35–50. https://doi.org/10.1016/j.jappgeo.2009.03.010

Farr, T. G., Rosen, P. A., Caro, E., Crippen, R., Duren, R., Hensley, S., et al. (2007). The shuttle radar topography mission. *Reviews of Geophysics*, *45*(2), RG2004. https://doi.org/10.1029/2005RG000183

Fialko, Y., Simons, M., & Agnew, D. (2001). The complete (3-D) surface displacement field in the epicentral area of the 1999 M_W 7.1 hector mine earthquake, California, from space geodetic observations. *Geophysical Research Letters*, *28*(16), 3063–3066. https://doi.org/10.1029/2001GL013174

Goldstein, R. M., & Werner, C. L. (1998). Radar interferogram filtering for geophysical applications. *Geophysical Research Letters*, *25*(21), 4035–4038. https://doi.org/10.1029/1998GL900033

Hu, J., Li, Z., Ding, X., Zhu, J., Zhang, L., & Sun, Q. (2012). 3D coseismic displacement of 2010 darfield, New Zealand earthquake estimated from multi-aperture InSAR and D-InSAR measurements. *Journal of Geodesy*, *86*(11), 1029–1041. https://doi.org/10.1007/s00190-012-0563-6

Ji, C., Helmberger, D. V., Wald, D. J., & Ma, K. F. (2003). Slip history and dynamic implications of the 1999 Chi-Chi, Taiwan, earthquake. *Journal of Geophysical Research*, *108*(B9). https://doi.org/10.1029/2002JB001764

King, G. C. P., Stein, R. S., & Lin, J. (1994). Static stress changes and the triggering of earthquakes. *Bulletin of the Seismological Society of America*, *84*(3), 935–953. https://doi.org/10.1785/BSSA0840030935

Kiser, E., & Ishii, M. (2017). Back-projection imaging of earthquakes. *Annual Review of Earth and Planetary Sciences*, *45*(1), 271–299. https://doi.org/10.1146/annurev-earth-063016-015801

Meade, B. J. (2007). Algorithms for the calculation of exact displacements, strains, and stresses for triangular dislocation elements in a uniform elastic half space. *Computers & Geosciences*, *33*(8), 1064–1075. https://doi.org/10.1016/j.cageo.2006.12.003

Mai, P. M., & Thingbaijam, K. K. S. (2014). SRCMOD: An online database of finite-fault rupture models. *Seismological Research Letters*, *85*(6), 1348–1357. https://doi.org/10.1785/0220140077

Maurin, T., Masson, F., Rangin, C., Min, U. T., & Collard, P. (2010). Collard P. First global positioning system results in northern Myanmar: Constant and localized slip rate along the Sagaing fault. *Geology*, *38*(7), 591–594. https://doi.org/10.1130/G30872.1

Meng, L., Inbal, A., & Ampuero, J. P. (2011). A window into the complexity of the dynamic rupture of the 2011 M_W 9 Tohoku-Oki earthquake. *Geophysical Research Letters*, *38*(7), L00G07. https://doi.org/10.1029/2011GL048118

Nikkhoo, M., & Walter, T. R. (2015). Triangular dislocation: An analytical, artefact-free solution. *Geophysical Journal International*, *201*(2), 1119–1141. https://doi.org/10.1093/gji/ggv035

Pasyanos, M. E., Masters, T. G., Laske, G., & Ma, Z. (2014). LITHO1. 0: An updated crust and lithospheric model of the Earth. *Journal of Geophysical Research: Solid Earth*, *119*(3), 2153–2173. https://doi.org/10.1002/2013JB010626

Stein, R. S. (1999). The role of stress transfer in earthquake occurrence. *Nature*, *402*(6762), 605–609. https://doi.org/10.1038/45144

Shiddiqi, H. A., Tun, P. P., & Ottemöller, L. (2019). Minimum 1D velocity model and local magnitude scale for Myanmar. *Seismological Research Letters*, *90*(5), 1923–1936. https://doi.org/10.1785/0220190065

Seber, G. A. F. & Wild, C. J. (Eds.) (1989)., *Nonlinear regression*. Wiley-Interscience.

Tukey, J. (1958). Bias and confidence in not quite large samples. *The Annals of Mathematical Statistics*, *29*(2), 614. https://doi.org/10.1214/aoms/1177706647

Wegmuller, U., & Werner, C. (1997). Gamma SAR processor and interferometry software. In *Paper presented at 3rd ERS symposium March 1997*.

Wang, X., Wei, S., Wang, Y., Maung Maung, P., Hubbard, J., Banerjee, P., et al. (2019). A 3-D shear wave velocity model for Myanmar region. *Journal of Geophysical Research: Solid Earth*, *124*(1), 504–526. https://doi.org/10.1029/2018JB016622

Erratum

Since original publication of this article, the first affiliation for coauthors Quanshu Zhao, Guoyan Jiang, Yingwen Zhao, Xiaoping Hu, Lei Yang, and Caijun Xu has been corrected as follows: School of Geodesy and Geomatics, School of Earth and Space Science and Technology, Wuhan University, Wuhan, China. The following affiliation has been deleted: School of Earth and Space Science and Technology, Wuhan University, Wuhan, China. This may be considered the authoritative version of record.